Supporting Information

NiFe prussian blue analogue cocatalyzed TiO_2/In_2S_3 type-II heterojunction for solar water splitting

Ming Zhang[1], Pingping Yang[2], Wenyan Tao[3], Xiangui Pang[2], Youyi Su[2], Pai Peng[2], Lin Zheng[2], Runhan Li[2], Shuxiang Wang[2], Jing Huang[2], Li Zou[2], Jiale Xie[2]

[1]School of Chemistry and Chemical Engineering, Southwest Petroleum University, Chengdu 610500, Sichuan, China.
[2]School of New Energy and Materials, Southwest Petroleum University, Chengdu 610500, Sichuan, China.
[3]Tongwei Solar Company, Chengdu 610299, Sichuan, China.

Correspondence to: Dr. Jiale Xie, School of New Energy and Materials, Southwest Petroleum University, 8 Xindu Road, Xindu District, Chengdu 610500, Sichuan, China.
E-mail: jialexie@swpu.edu.cn

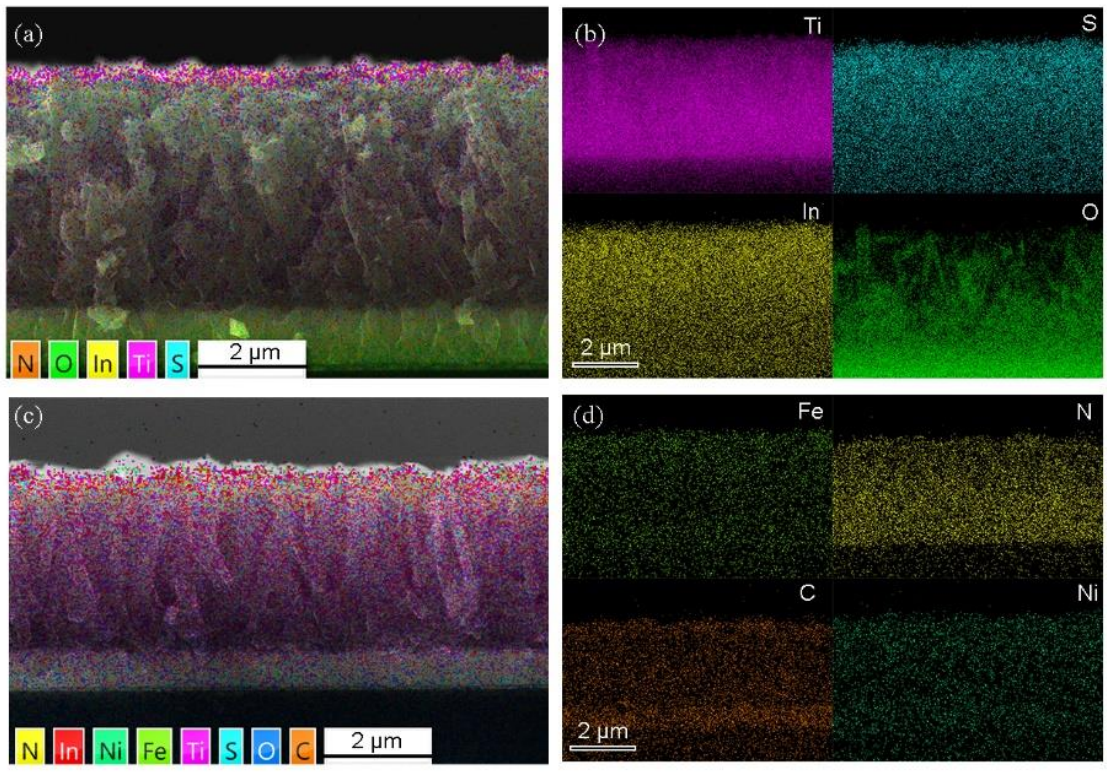

Figure S1. EDS images of TiO_2/In_2S_3 (a, b) and TiO_2/In_2S_3/NFP (c, d).

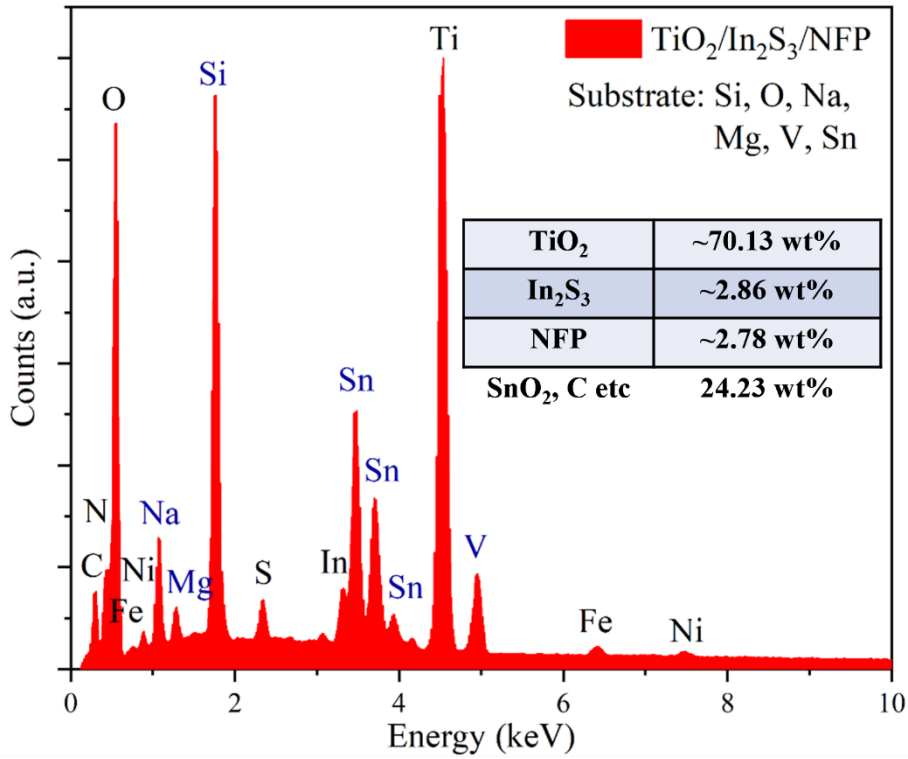

Figure S2. EDS pattern of TiO_2/In_2S_3/NFP photoanode.

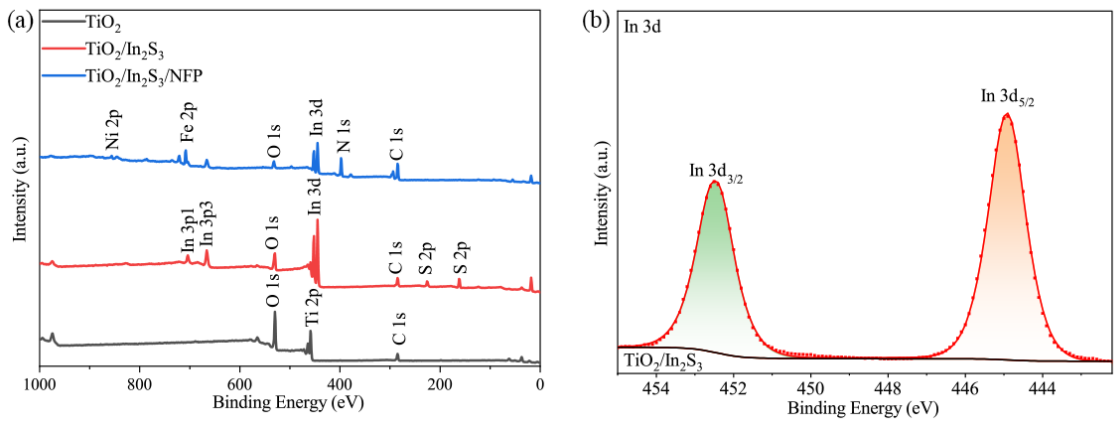

Figure S3. (a) XPS survey spectra of TiO_2, TiO_2/In_2S_3, and TiO_2/In_2S_3/NFP. (b) XPS spectra of In 3d of TiO_2/In_2S_3 photoanode.

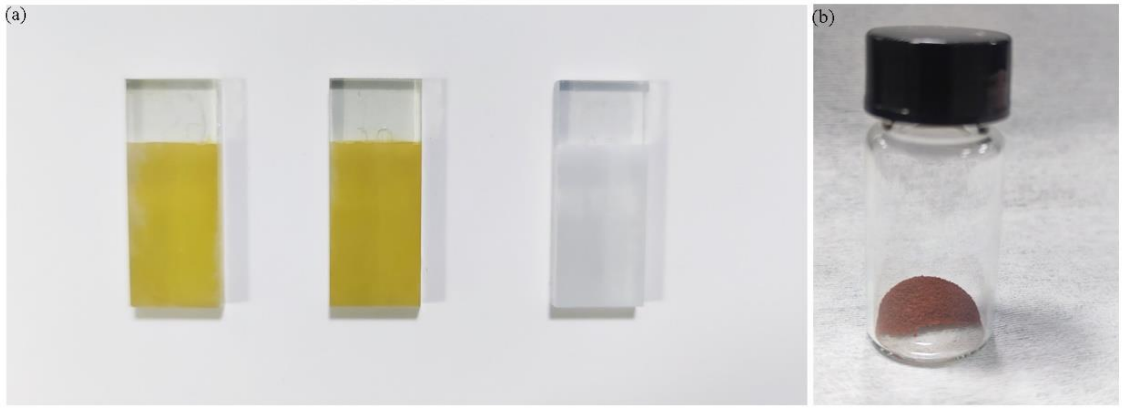

Figure S4. (a) Optical images of TiO_2 (right), TiO_2/In_2S_3 (left), and TiO_2/In_2S_3/NFP (middle) photoanodes. (b) Optical image of as-prepared In_2S_3 powder.

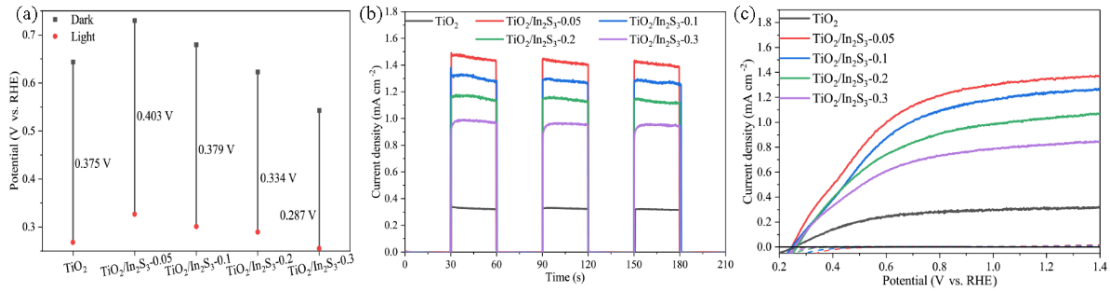

Figure S5. Photovoltage (a), it (b), LSV (c) curves of TiO_2/In_2S_3 with different precursor concentrations.

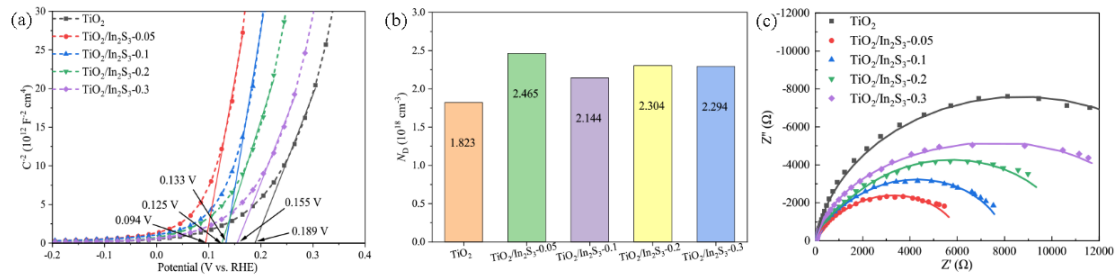

Figure S6. (a) M-S plots of TiO_2 and TiO_2/In_2S_3 photoanodes measured at 2000 Hz in the dark. (b) Histogram of the corresponding carrier concentration. (c) Nyquist plots of TiO_2-based photoanodes measured at 0.47 V *vs.* RHE under AM1.5G illumination.

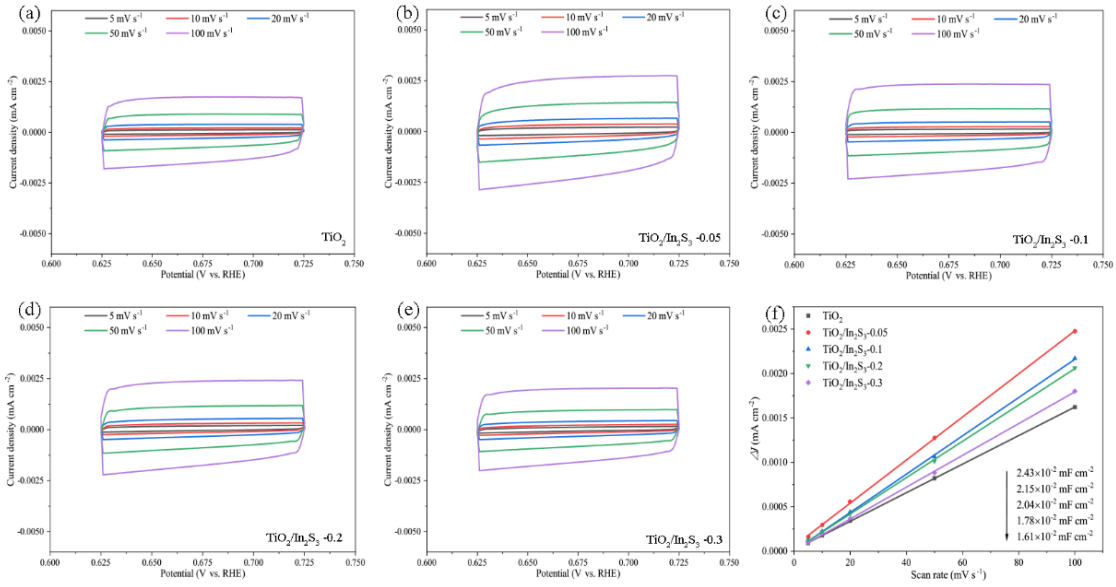

Figure S7. CV curves of TiO_2 (a) and TiO_2/In_2S_3 (b-e) prepared with different precursor concentrations in 1 M KOH at a scan rate of 5-100 mV s^{-1}. (f) Determination of capacitance (C_{dl}) values through ΔJ *vs.* scan rate plots for TiO_2-based photoanodes.

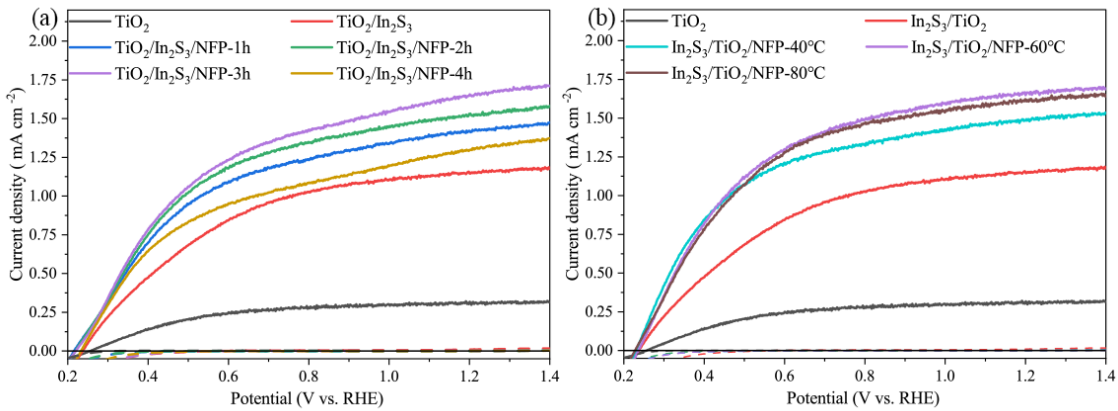

Figure S8. LSV curves of TiO_2/In_2S_3/NFP at different reaction times (a) and various reaction temperatures (b).

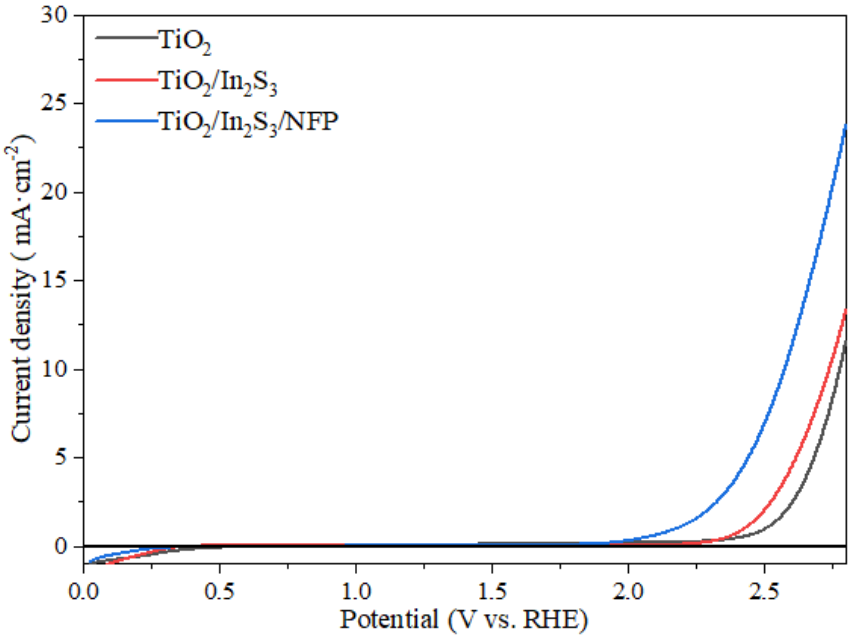

Figure S9. Dark LSV curves of TiO_2, TiO_2/In_2S_3, and TiO_2/In_2S_3/NFP electrodes measured at a scan rate of 20 mV s^{-1}.

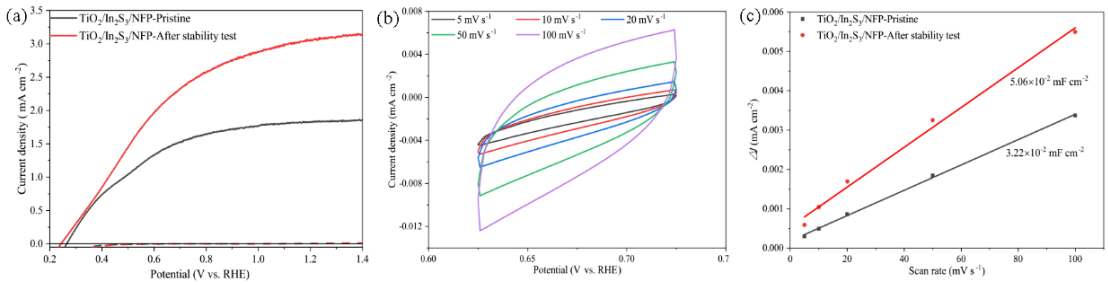

Figure S10. LSV (a) and CV (b) curves of TiO_2/In_2S_3/NFP photoanode before and after stability testing. (c) Determination of capacitance (C_{dl}) values through ΔJ *vs.* scan rate plots for TiO_2/In_2S_3/NFP photoanode before and after stability testing.

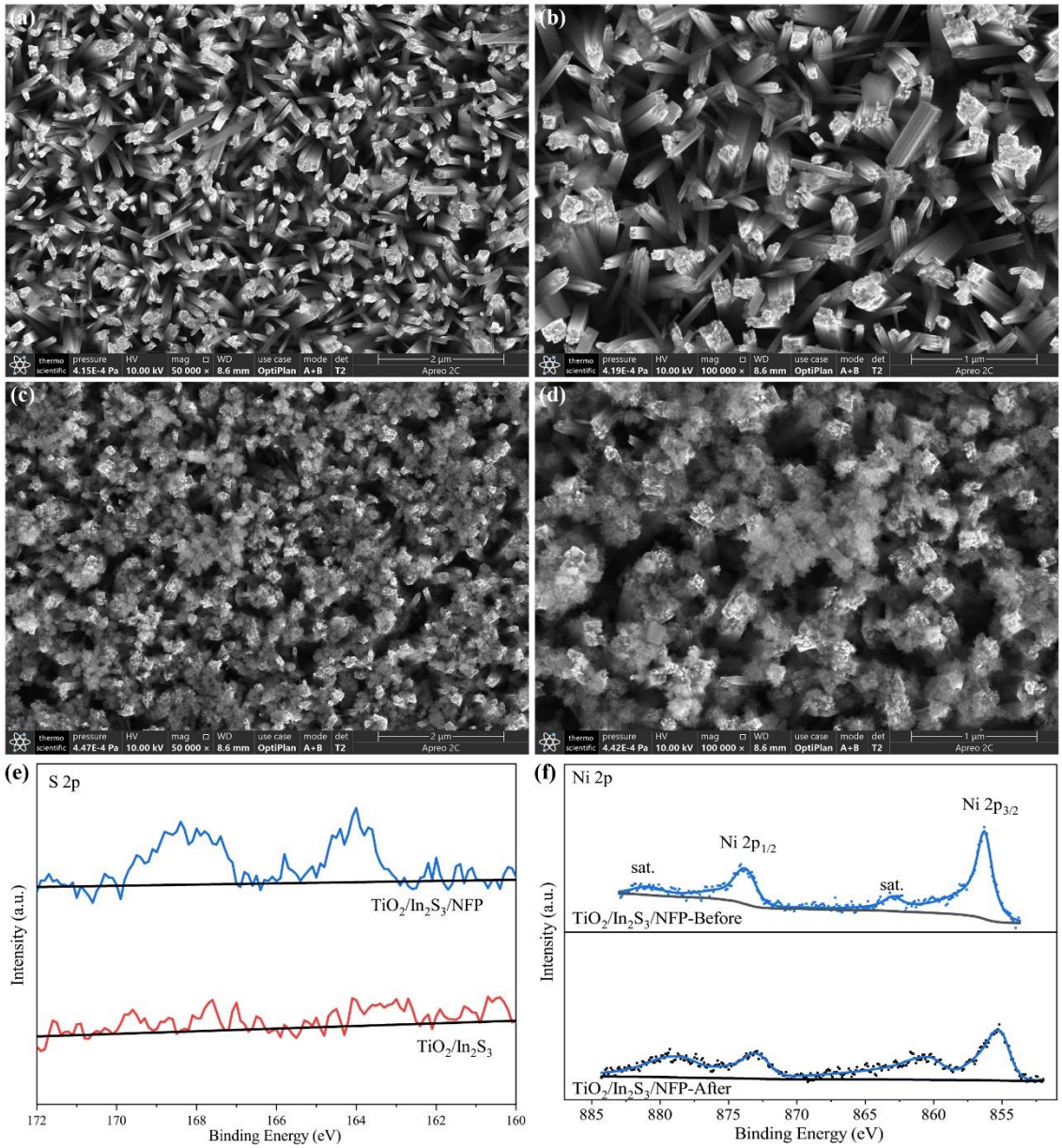

Figure S11. (a, b) SEM images of TiO_2/In_2S_3 photoanode after the stability test. (c, d) SEM images of TiO_2/In_2S_3/NFP photoanode after the stability test. (e) S 2p XPS spectra of the tested TiO_2/In_2S_3 and TiO_2/In_2S_3/NFP photoanodes. (f) Ni 2p XPS spectra of the as-prepared and tested TiO_2/In_2S_3/NFP photoanodes.

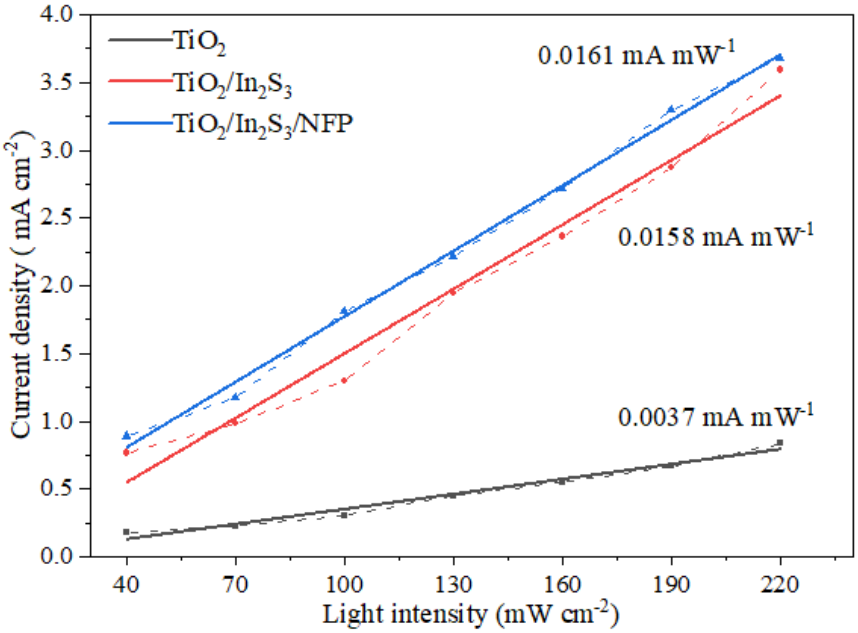

Figure S12. Relationship of photocurrent density *vs.* light intensity of TiO_2, TiO_2/In_2S_3, and TiO_2/In_2S_3/NFP photoanodes.

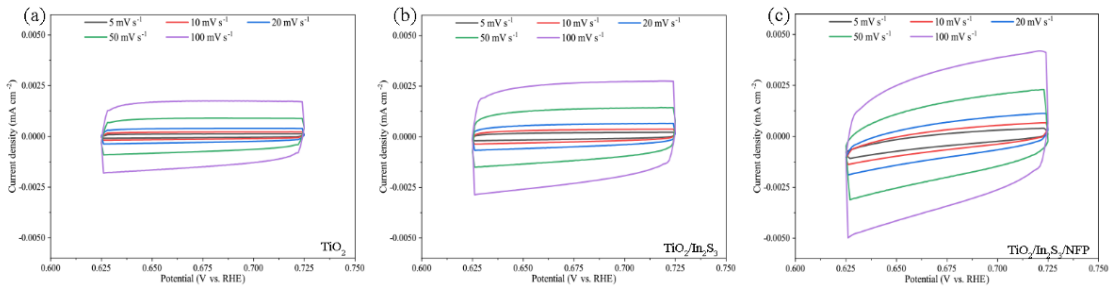

Figure S13. CV curves of TiO_2 (a), TiO_2/In_2S_3 (b), and TiO_2/In_2S_3/NFP (c) in 1 M KOH at a scan rate of 5-100 mV s^{-1}.

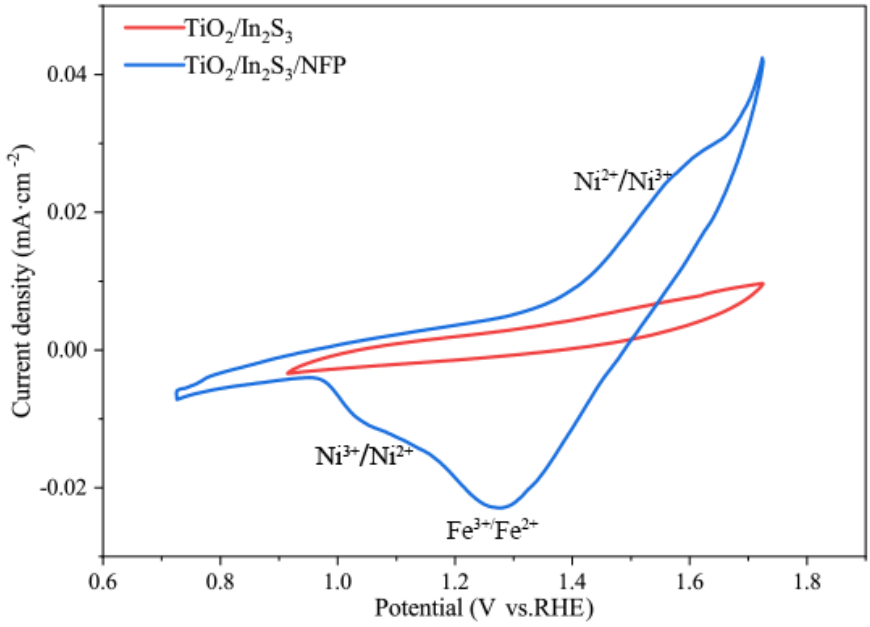

Figure S14. CV curves of TiO_2/In_2S_3 and TiO_2/In_2S_3/NFP electrodes measured at a scan rate of 20 mV s^{-1} and in the dark.

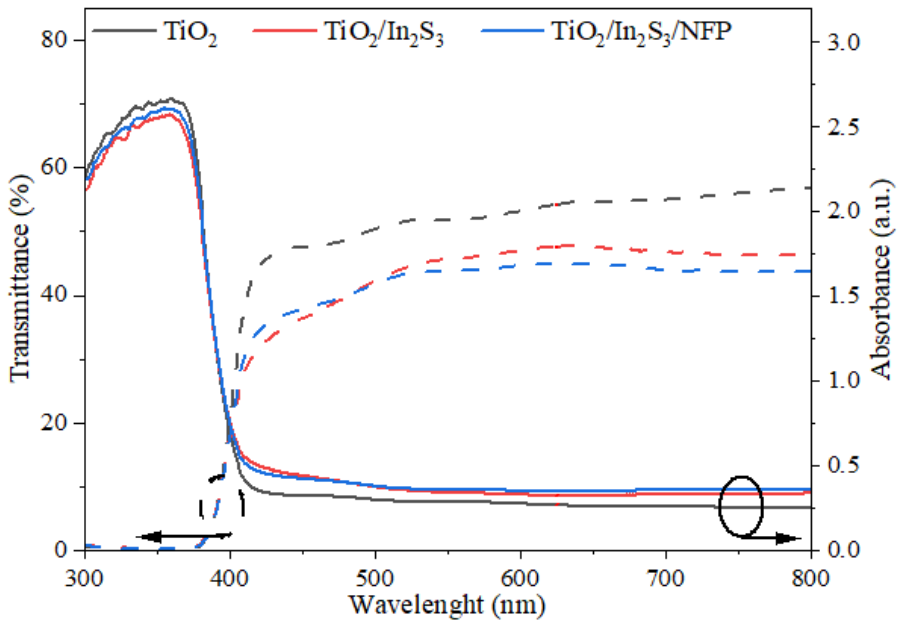

Figure S15. Transmission spectra and UV-vis absorption spectra of TiO_2, TiO_2/In_2S_3, and TiO_2/In_2S_3/NFP photoanodes.

The bandgap (E_g) and the theoretical photocurrent density (J_{abs}) of TiO_2-based films are obtained by:

$$(\alpha h\nu)^{1/n} = A(h\nu - E_g) \quad \text{(S1)}$$

$$J_{abs} = \frac{1}{E_g}\int_{\lambda_2}^{\lambda_1} A_\lambda \ \Phi_\lambda d\lambda \quad \text{(S2)}$$

where α denotes the absorbance index, h represents the Planck constant, v signifies the frequency of light, A stands for a material-specific constant, E_g represents the band gap of the semiconductor, A_λ characterizes the absorption rate of the semiconductor photocathode, and Φ_λ delineates the photon flux within the AM1.5G spectrum.

Table S1. Comparison of the performance of this work with the reported related photoanodes.

Photoanode	**Electrolyte (AM 1.5G)**	***J* (mA cm^{-2}) (1.23 V vs. RHE)**	**Stability**	**Ref.**
S,N-TiO_2/In_2S_3	1 M NaOH	2.74 mA cm^{-2}, 3.5 times	20 h, 80%	[1]
FTO/TiO_2/In_2S_3	Na_2S/Na_2SO_3	1.74 mA cm^{-2} (0 V *vs.* Ag/AgCl)	6 h, 86.4%	[2]
TiO_2/In_2S_3	1 M $Na_2S_2O_3$	1.1 mA cm^{-2}	N/A	[3]
GO/In_2S_3/TiO_2	0.5 M Na_2SO_4	0.2 mA cm^{-2}, 20 times (0 V *vs.* Ag/AgCl)	1000 s, ~76%	[4]
V-TiO_2@β-In_2S_3	0.25 M Na_2S + 0.35 M Na_2SO_3	1.42 mA cm^{-2}, 3 times (0.5 V *vs.* Ag/AgCl)	2000 s	[5]
Fe_2O_3/Fe_2TiO_5/CoFe-PBA	0.1 M $NaNO_3$ + 0.1 M HNO_3	1.25 mA cm^{-2}	24 h, 80%	[6]
ZnO/$BiVO_4$/NiFePB	0.5 M Na_2SO_4	1.66 mA cm^{-2}	N/A	[7]
TiO_2@FeFe-PB	0.1 M Na_2SO_4	1.5 mA cm^{-2}, 2 times	2400 s, 80%	[8]
CoFe-PBA/PiH	1 M NaOH	1.24 mA cm^{-2}	N/A	[9]
α/γ-Fe_2O_3/FCP	1 M KOH	3.5 mA cm^{-2}, 7.8 times	2h, 94%	[10]
TiO_2/[CoFe–JG]	0.1 M PBS, pH=7	551 μA cm^{-2}	2 h, 80%	[11]
$CoFe(OH)_x$@Sb-TiO_2	0.5 M Na_2SO_4	1.48 mA cm^{-2}	N/A	[12]
TiO_2/In_2S_3/NFP	1 M KOH	1.81 mA cm^{-2}, 6 times	12 h, 95.17%	This work

REFERENCES

1. Park J, Lee TH, Kim C et al. Hydrothermally obtained type-II heterojunction nanostructures of In_2S_3/TiO_2 for remarkably enhanced photoelectrochemical water splitting. *Appl Catal B Environ*. 2021;295:120276. [DOI: 10.1016/j.apcatb.2021.120276]

2. Hsieh PY, Chiu YH, Lai TH et al. TiO_2 Nanowire-Supported Sulfide Hybrid Photocatalysts for Durable Solar Hydrogen Production. *ACS Appl Mater Interfaces*. 2019;11:3006-3015. [DOI: 10.1021/acsami.8b17858]

3. Wang X, Li H, Zhang J, Liu X, Zhang X. Wedged β-In_2S_3 sensitized TiO_2 films for enhanced photoelectrochemical hydrogen generation. *J Alloys Compd*. 2020;831:154798. [DOI: 10.1016/j.jallcom.2020.154798]

4. Braiek Z, Ben Naceur J, Jrad F, Ben Assaker I, Chtourou R. Novel synthesis of graphene oxide/In_2S_3/TiO_2 NRs heterojunction photoanode for enhanced photoelectrochemical (PEC) performance. *Int J Hydrog Energy*. 2022;47:3655-3666. [DOI: 10.1016/j.ijhydene.2021.10.268]

5. Mumtaz A, Mohamed NM, Mazhar M, Ehsan MA, Mohamed Saheed MS. Core–Shell Vanadium Modified Titania@β-In_2S_3 Hybrid Nanorod Arrays for Superior Interface Stability and Photochemical Activity. *ACS Appl Mater Interfaces*. 2016;8:9037-9049. [DOI: 10.1021/acsami.5b10147]

6. Tang P, Han L, Hegner FS et al. Boosting Photoelectrochemical Water Oxidation of Hematite in Acidic Electrolytes by Surface State Modification. *Adv Energy Mater*. 2019;9:1901836. [DOI: 10.1002/aenm.201901836]

7. Bai S, Jia S, Zhao Y et al. NiFePB-modified ZnO/$BiVO_4$ photoanode for PEC water oxidation. *Dalton Trans*. 2023;52:5760-5770. [DOI: 10.1039/d3dt00013c]

8. Mao G, Li C, Li Z et al. Efficient charge migration in TiO_2@PB nanorod arrays with core–shell structure for photoelectrochemical water splitting. *CrystEngComm*. 2022;24:2567-2574. [DOI: 10.1039/d1ce01710a]

9. Khan AZ, Kandiel TarekA, Abdel-Azeim S, Jahangir TN, Alhooshani K. Phosphate ions interfacial drift layer to improve the performance of CoFe−Prussian blue hematite photoanode toward water splitting. *Appl Catal B Environ*. 2022;304:121014. [DOI: 10.1016/j.apcatb.2021.121014]

10. Li Y, Chen Y, Wu Q et al. Revealing long-lived electron–hole migration in core–shell α/γ-Fe_2O_3/FCP for efficient photoelectrochemical water oxidation. *Catal Sci Technol*.

2022;12:250-258. [DOI: 10.1039/D1CY01628H]

11. Ulusoy Ghobadi TG, Ghobadi A, Buyuktemiz M et al. A Robust, Precious-Metal-Free Dye-Sensitized Photoanode for Water Oxidation: A Nanosecond-Long Excited-State Lifetime through a Prussian Blue Analogue. *Angew Chem Int Ed*. 2020;59:4082-4090. [DOI: 10.1002/anie.201914743]

12. Pal D, Maity D, Sarkar A et al. Multifunctional Ultrathin Amorphous CoFe-Prussian Blue Analogue Catalysts for Efficiently Boosting the Oxygen Evolution Activity of Antimony-Doped TiO_2 Nanorods Photoanode. *ACS Appl Energy Mater*. 2022;5:15000-15009. [DOI: 10.1021/acsaem.2c02608]